

Magnetism of Fullerene C₆₀ Compared with Graphene Molecule by DFT Calculation, Laboratory Experiment and Astronomical Observation

Norio Ota¹, Aigen Li², Laszlo Nemes³ and Masaaki Otsuka⁴

¹Graduate school of Pure and Applied Sciences, University of Tsukuba, 1-1-1 Tennodai, Tsukuba-City Ibaraki, 305-8571, Japan

²Department of Physics and Astronomy, University of Missouri, Columbia, MO 65211, USA,

³Research Center for Natural Sciences, Ötvös Lóránd Research Network, Budapest 1519, Hungary

⁴Okayama Observatory, Kyoto University, Asakuchi Okayama, 719-0232, Japan.

Magnetism of fullerene C₆₀ was studied by three methods of the density functional theory (DFT) calculation, laboratory experiment and astronomical observation. DFT revealed that the most stable spin state was non-magnetic one of $S_z=0/2$. This is contrary to our recent study on void induced graphene molecules of C₂₃ and C₅₃ to be magnetic one of $S_z=2/2$. Two graphene molecules combined model suggested that two up-spin at every carbon pentagon ring may cancel each other to bring $S_z=0/2$. Similar cancelation may occur on C₆₀. Molecular vibrational infrared spectrum of C₆₀ show four major bands, which coincide with gas-phase laboratory experiment, also with astronomically observed one of carbon rich planetary nebula Tc1 and Lin49. However, there remain many unidentified bands on astronomical one. We supposed multiple voids on graphene sheet, which may create both C₆₀ and complex graphene molecules. It was revealed that spectrum of two voids induced graphene molecule coincident well with major astronomical bands. Simple sum of C₆₀ and graphene molecules could successfully reproduce astronomical bands in detail.

Key words: fullerene C₆₀, graphene, DFT, gas-phase experiment, planetary nebula, infrared spectrum

1. Introduction

Graphene and graphite like carbon materials are candidates for showing ferromagnetic like hysteresis¹⁻⁶. There are many capable explanations based on impurities⁷, edge irregularities⁸⁻¹⁰ or defects¹¹⁻¹⁷. The density functional theory (DFT) shows good coincidence with experiments¹⁸⁻²¹ and revealed reasonable consistency with several fundamental theories²²⁻²³. Despite such many efforts, origin of magnetic ordering could not be thoroughly understood. Our recent studies on graphene nano-ribbon (GNR)¹⁷ and on graphene molecules²⁴ revealed that void-defect brings unusual highly polarized spin configuration and structure change. Especially on graphene molecules²⁴, we could firstly suggest good coincidence of DFT calculated molecular vibrational infrared spectrum both with astronomical observation of carbon rich planetary nebula²⁵, and with laboratory experiment of laser induced carbon plasma²⁶. Model molecules for DFT calculation were graphene molecules of C₂₃ and C₅₃ induced by single void-defect. They have one carbon pentagon ring combined with many hexagon rings. Single void has three radical carbons, holding six spins. Those spins make several spin-states, which affects to molecular structure and molecular vibration, finally to infrared spectrum.

It was amazing that the stable spin state was magnetic one of spin state $S_z=2/2$, not non-magnetic one of $S_z=0/2$. Here, there is an interesting question that fullerene C₆₀ is magnetic or not. Fullerene has 12 carbon pentagon rings combined with 20 hexagons, which is similar combination with void-induced graphene molecules. In this paper, we like to study magnetism of C₆₀ by three methods of DFT calculation, laboratory experiment^{27, 28}, and astronomical observation²⁵. Comparison with astronomical infrared spectrum is important that DFT calculates isolate and zero temperature status molecule. Also, astronomical carbon dust is similar situation, floating in interstellar space under ultra-low density (1~100 molecules/cm³) and low temperature (few to 10 K) conditions.

Fullerene C₆₀ was discovered by Kroto et al.³⁰ (the 1996 Nobel Prize) in the sooty residues of vaporized carbon. They already suggested that “fullerene may be widely distributed in the universe”. The presence of C₆₀ in astrophysical environments was revealed by the detection of a set of emission bands at 7.0, 8.45, 17.3 and 18.9 μm ³¹⁻³⁷. Typical astronomical objects are the Galactic planetary nebula (PNe) Tc1³¹ and the Small Magellanic Cloud PNe Lin49²⁵. Observed spectra were compared with experiment and theory³⁸⁻⁴⁰. However, there remain undetermined observed bands, cannot be explained only by C₆₀.

It is well known that graphene is a raw material for synthesizing fullerene^{39, 40}. By observation of Lin49, Otsuka et al.²⁵ suggested the presence of small

Corresponding author: Norio Ota (n-otajitaku@nifty.com).

graphene. Graphene was first experimentally synthesized by Geim and Novoselov⁴¹⁾ (the 2010 Nobel Prize). The possible presence of graphene in space was reported by Garcia-Hernandez et al.⁴²⁻⁴⁴⁾. These infrared features appear to be coincident with planar C₂₄ having seven carbon hexagon rings. However, full observed bands still cannot be explained by C₂₄ or hexagon network molecules⁴⁵⁾. Some hints come from carbon SP₃ defect among SP₂ network caused by void-defect in carbon hexagon network by Ota⁴⁶⁾. Also, Galue & Leines⁴⁷⁾ predicted the physical model supposing pi-electron irregularity. Resulted molecular configuration was carbon pentagon rings among hexagon networks.

At first part of this paper, stable spin state and vibrational infrared spectrum of C₆₀ will be calculated and compared with laboratory experiments and astronomical observation. Those will be compared with single-void induced graphene C₂₃ and C₅₃. At second part, multiple-void induced graphene molecules as like C₂₂, C₂₁, C₅₂ and C₅₁ will be calculated, which results are compared with that of fullerene C₆₀.

2. Calculation Method

In calculation, we used DFT^{48/49)} with the unrestricted B3LYP functional⁵⁰⁾. We utilized the Gaussian09 software package⁵¹⁾ employing an atomic orbital 6-31G basis set⁵²⁾. Unrestricted DFT calculation was done to have the spin dependent atomic structure. The required convergence of the root-mean-square density matrix was 10⁻⁸. Based on such optimized molecular configuration, fundamental vibrational modes were calculated, such as carbon to carbon (C-C) stretching modes, C-C bending modes and so on, using the Gaussian09 software package. This calculation also gives harmonic vibrational frequency and intensity in infrared region. The standard scaling is applied to the frequencies by employing a scale factor of 0.975 for pure carbon system taken from the laboratory experimental value of 0.965 based on coronene-molecule of C₂₄H₁₂⁴⁶⁾. Correction due to anharmonicity was not applied to avoid uncertain fitting parameters. To each spectral line, we assigned a Gaussian profile with a full width at half maximum (FWHM) of 4cm⁻¹.

It should be noted that any molecular symmetry was not applied to compare delicate change of molecular configuration and compare small difference of total energy.

3. Spin State Analysis of Fullerene C₆₀

3.1 Stable spin state of C₆₀ compared with graphene molecule.

For DFT calculation of C₆₀, input condition is charge neutral for two cases of spin state of $S_z=0/2$ or $S_z=2/2$.

In this study, we dealt total molecular spin \mathbf{S} (vector). Molecule is rotatable material, easily follows to the external magnetic field of z-direction. Projected component S_z to z-direction is good quantum number.

Result is shown in Fig. 1. Total molecular energy of $S_z=0/2$ is 1.79 eV lower (stable) than that of $S_z=2/2$, that is, C₆₀ is not magnetic and show no spin-distribution. Spin-density of $S_z=2/2$ was mapped on right bottom, of which up-spin cloud (by red) surrounds around an equator of soccer ball like C₆₀. Such excess up-spin cloud of $S_z=2/2$ brings slight energy increase than $S_z=0/2$.

Stable spin state of C₆₀ was contrary to our previous study on single-void-defect induced graphene molecules of C₂₃ which show stable spin state to be $S_z=2/2$ ²⁴⁾. Typical example was illustrated in Fig. 2. Starting molecule was C₂₄ having seven carbon hexagon rings. High-speed particle attacks one carbon atom and kick out. Single void will be created. DFT calculation gives optimized molecular configuration. Resulted molecule was C₂₃ having one pentagon ring. In our previous paper²⁴⁾, we named (C₂₃-c) to distinguish void position. Initial void-defect holds 3 radical carbons and allows 6 spins. Six spins make capable spin-states of $S_z=0/2, 2/2, 4/2$ and $6/2$. Among them, calculated energy of $S_z=4/2$ and $6/2$ resulted unstable high energy. Here, we should compare cases of $S_z=0/2$ and $2/2$. It should be noted that molecular energy of $S_z=2/2$ was 0.64 eV lower (stable) than that of $S_z=0/2$. We can see up-spin major spin cloud for $S_z=2/2$ on bottom right at a cutting surface of spin density at 10e/nm³.

Molecular vibrational infrared bands of C₆₀ were shown in Table 1, for $S_z=0/2$ in column (d) and for $S_z=2/2$ in (e). Fundamental vibrational mode of $S_z=0/2$ were noted in (d). We noticed four major bands. Mode of Band-A (18.72 μm) was C-C stretching on C₆₀ surface fixing carbon to carbon length of pentagon ring. Mode of Band-B (17.44 μm) was asymmetric spherical motion of C₆₀ ball. Modes of Band-C (8.58 μm) and Band-D (6.77 μm) were both C-C stretching on C₆₀ surface.

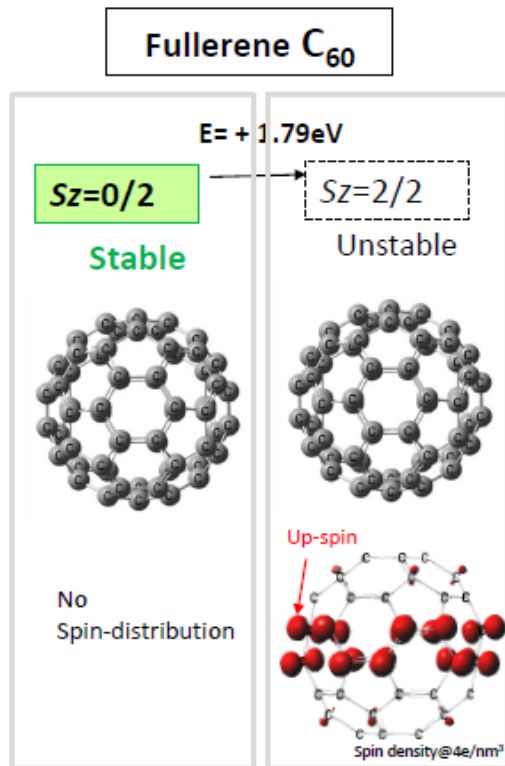


Fig. 1 Spin state of fullerene C₆₀ by DFT calculation.

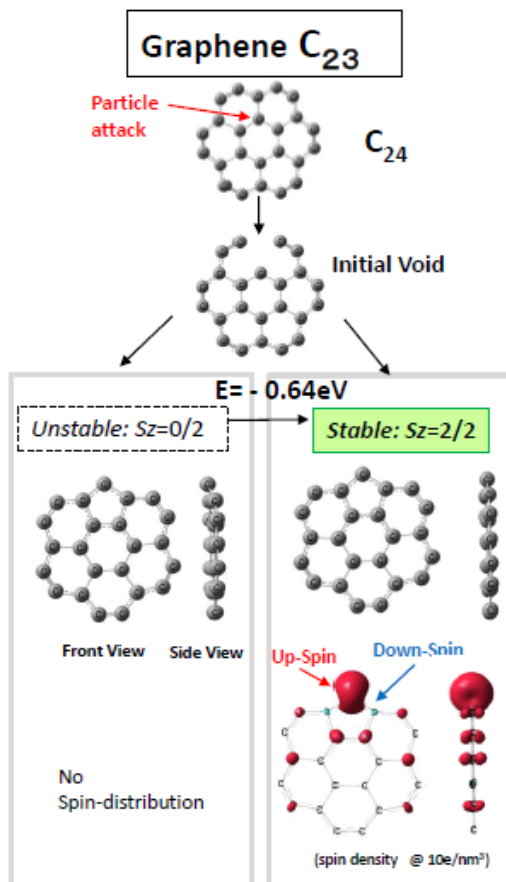


Fig. 2 Spin state of single void induced graphene C₂₃.

3.2 Spin alignment of C₆₀

It should be noted that stable spin state of C₆₀ is $Sz=0/2$. This is contrary to that of C₂₃ and C₅₃. To understand such difference, we consider simple spin alignment model as shown in Fig. 3. Two molecules of C₂₃ were supposed as illustrated on column (A). As shown on right, if two carbon atoms (1C, 2C) of each carbon pentagon rings (marked by circled 5) were far enough, there remains original up-spin cloud as up-up pair. Coupled molecules may show total spin of $Sz=4/2$. Whereas as shown on left, two molecules were close enough, two molecules will make a new bond. Spin alignment will be up-down pair to result $Sz=0/2$. Such new covalent bond will reduce total energy. Under such consideration, we can suggest two capabilities of C₆₀ as shown on panel (B), that is, non-magnetic one on left and magnetic one on right. By DFT calculation, we could obtain precise molecular configuration on (C) and could judge preferable spin state to be $Sz=0/2$.

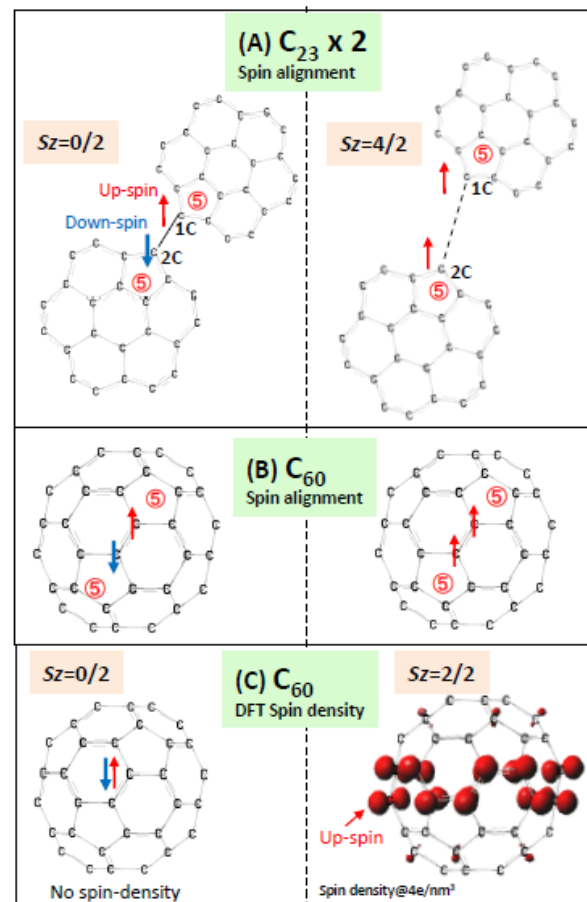


Fig. 3 Spin alignment model by two graphene molecules of C₂₃ was illustrated in (A), analogy to C₆₀ in (B). DFT calculated spin distribution of C₆₀ was shown in (C).

Table 1 Molecular vibrational bands of fullerene C₆₀.

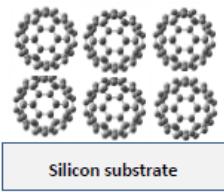
	C60: Laboratory Experiment			C60: DFT Calculation	
	(a) Gas-phase (~1000 K) [Nemes et al.]	(b) Gas-phase (Extrapolate to 0 K) [Nemes et al.]	(c) Solid-phase (300 K) [Kratschmer et al.]	(d) Sz=0/2 (Stable) [This study]	(e) Sz=2/2 (Unstable) [This study]
Remarks	Gas-phase experiment	Extrapolation to 0 K	Solid-phase experiment	Isolate C60 at zero-temperature	
Material phase	 (Gas-phase, 1000-> 0 K)		 (Solid-phase, 300 K)	 (Isolate , 0 K)	
Band- A	18.95	18.82	18.93	18.72 (C-C stretching on C60- surface fixing pentagon ring's carbon to carbon length)	18.71
Band- B	17.54	17.41	17.33	17.44 (Asymmetric spherical motion of C60 ball)	17.68
Infrared band (micrometer)					13.71
					13.35
Band- I	8.58	8.40	8.45	8.58 (C-C stretching on C60-surface)	
Band- L	7.11	6.97	7.00	6.77 (C-C stretching on C60-surface)	7.00

Table 2 Vibrational bands of graphene molecules.

Laboratory Experiment			Astronomical Observation		DFT Calculation (0 K, Isolate molecule)							
C60 Gas-phase (Extrapolated to 0 K)	C60 Solid (300K)	Laser induced carbon (300K)	Tc1 Nebula	Lin49 Nebula	C60 Sz=0/2	C24 Sz=0/2	C23 Sz=2/2	C22 Sz=2/2	C21 Sz=4/2	C53 Sz=2/2	C52 Sz=2/2	C51 Sz=2/2
Number of carbon rings hexagon: 20 pentagon: 12	-	-			20 12	7 0	6 1	5 2	4 3	18 1	17 2	16 3
(Wavelength in micrometer)						20.1		19.8			19.6	19.1
18.93			18.9 μm	18.9			19.1	19.2		18.9	18.9	
18.82					18.72		18.9	19.0				18.6
17.41	17.33		17.4	17.4	17.44		17.4	17.3	17.4			
				16.6			16.9	16.5				
				14.3			14.3	16.4		14.3		
				13.9						13.9	13.8	13.5
				13.3					12.7	13.4	13.3	13.1
		10.2		10.0			9.9	10.2			11.4	
		9.5				9.8	9.0	8.9	8.9		9.3	9.0
8.40	8.45		8.4	8.4	8.58					8.6	8.4	8.3
		8.3		8.1			8.0	8.1	7.9			
		7.7	7.6	7.6				7.5	7.6	7.6	7.6	7.6
		7.4					7.4			7.3		
6.97	7.00	Plateau (5.9-7.7)	7.1	7.1			7.1		7.2	7.1	7.1	7.0
		6.7	6.5	6.6	6.77	6.6	6.6	6.6		6.5	6.3	6.5
		5.9								6.3	6.3	

3.3 Comparison with laboratory experiments

There are several laboratory experiments of infrared emission bands of C_{60} as summarized on Table 1. In a column (c), emission bands of solid phase C_{60} clusters, stucked on silicon substrate, was measured at 300 K by Kratschmer et al.²⁸⁾, which show four bands at 18.93, 17.33, 8.45 and 7.00 μm . Solid-phase experiment has an advantage to give sufficient strong emission signal. DFT calculated bands (d) were close to those bands within 0.2 μm discrepancy. However, we should mind that molecular motion of solid phase would be bound by neighbor molecules and by silicon substrate. Gas-phase experiments is necessary to obtain near isolate and motion free emission spectrum. Nemes et al.²⁷⁾ show high temperature (879~1212 K) emission bands as noted in (a) to be 18.95, 17.54, 8.58, and 7.11 μm , which show longer wavelength than solid-phase one. To compare DFT calculation, low temperature behavior is necessary, but emission intensity is so weak. They simply extrapolated to 0 K based on high temperature experiment as shown in (b), where Band-A, is 18.82 μm close to DFT obtained 18.72 μm (d). Band-B just coincide well each other at 17.4 μm . Band-C show 8.40 μm (b) compared to DFT calculated 8.58 μm (d). Also, Band-D was 6.97 μm (b) compared to calculated 6.77 μm (d). They show reasonable coincidence within 0.2 μm discrepancy.

3.4 Comparison with astronomically observed infrared-spectrum

Comparison of DFT calculation with astronomically observed bands is important, because they are both ideal cases of ultra-low material density and at low temperature. Otsuka et al.²⁵⁾ opened astronomically observed bands as illustrated in Fig. 4, on top for Tc1 nebula by red and for Lin49 nebula by blue. On middle, gas-phase zero-temperature extrapolated bands of C_{60} were marked by blue arrows. DFT calculated spectra were illustrated on bottom for the case of $Sz=0/2$ by green and for $Sz=2/2$ by light green. It should be noted that the observed spectra are seen in emission. A nearby star as like a central star of Tc1 nebula may illuminate the molecules and excites them to give rise infrared emission. Detailed discussion was done by Li and Drain^{53),54)}. We regard that DFT calculated absorbed spectrum is mirror image of emission one in case of sufficient large photon energy excitation due to the theory of Einstein's emission coefficient^{53),54)}.

Calculated spectrum of $Sz=2/2$ (by light green) was so different with astronomical one. On the other hand, spectrum of $Sz=0/2$ (by green) looks good to reproduce astronomical one. Band behavior is ambiguous for $Sz=2/2$. Energy favorable spin state of $Sz=0/2$ show specific four bands. Both Tc1 and Lin49 show major band at 18.9 μm , which is only 0.1 μm longer than gas-phase experimental one, and 0.2 μm longer than

DFT calculated one of C_{60} . It looks fair coincidence. Sharp emission at 18.7 μm (marked by black arrow) is a strong atomic emission line of S_{III} . We are afraid that such strong atomic emission may hide true molecular band of C_{60} . DFT calculated Band-B (17.44 μm) coincides so well both with astronomically observed one and with gas-phase laboratory experimental one. In shorter wavelength region, calculated C_{60} has two bands at 8.58 and 6.77 μm . It looks fair coincidence with gas-phase experimental bands at 8.40 and 6.97 μm , also with astronomically observed one at 8.4 and 6.6 μm .

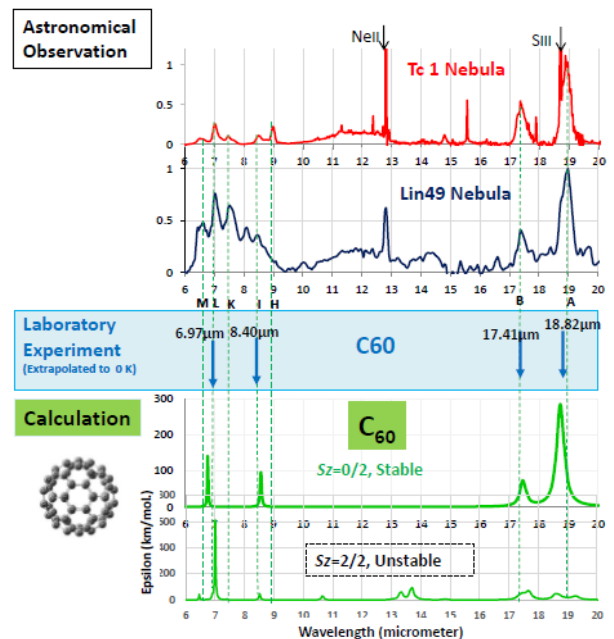


Fig. 4 Comparison of molecular vibrational infrared spectra on fullerene C_{60} by astronomical observation, by laboratory experiment and by DFT spin dependent calculations.

It should be noted that there are many unidentified astronomical bands. Those complex bands may come from unknown carbon molecules, not only by single molecule of C_{60} . Our previous study²⁴⁾ considered single void-defect on mother graphene of C_{24} and C_{54} . Resulted graphene were C_{23} and C_{53} , which infrared spectra are again illustrated in Fig. 5 and Table 2. Major band of C_{23} has twin peaks at 18.9 and 19.0 μm , also C_{53} has single peak at 18.9 μm , which are related to observed Band-A. Second major observed band was at 17.4 μm (Band-B), which was reproduced well by C_{60} . Unfortunately, Band-B was reproduced by C_{23} and C_{53} only by weak intensity band. At shorter wavelength region from 6 to 10 μm , spectrum of C_{60} only show two bands of Band-I and -L, while C_{23} and C_{53} could reproduce many bands as like G, H, I, J, K, L and M. Moreover, C_{53} could reproduce detailed bands of D, E, F. In Table 2, Nemes et al. reported another

laboratory experiment by the laser induced carbon plasma^{24),26)}. We can see rough coincidence with bands from graphene molecules, little coincidence with C₆₀.

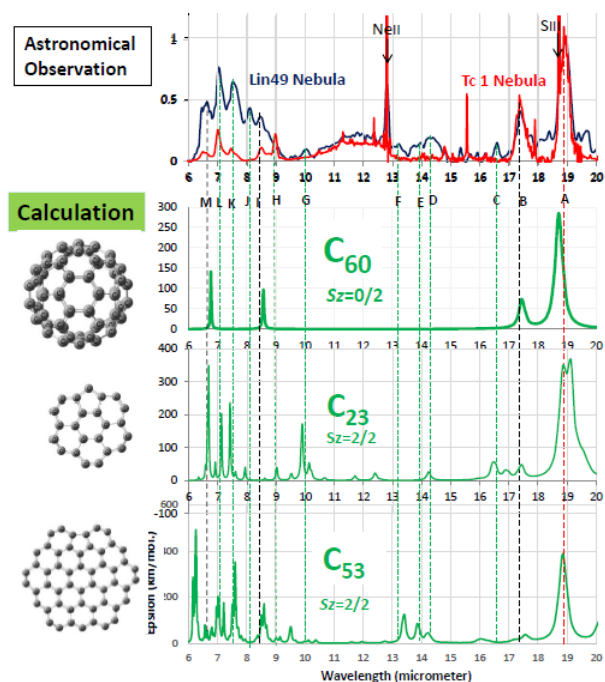


Fig. 5 DFT calculated molecular vibrational spectra of (C₆₀, $Sz=0/2$), (C₂₃, $Sz=2/2$) and (C₅₃, $Sz=2/2$) compared with astronomically observed spectra of carbon rich nebulae Tc1 and Lin49.

4. Multiple-Void Induced Carbon Molecules

4.1 The top-down process

It should be noted that infrared spectrum of C₆₀ show strong band at 17.4 μm (Band-B), whereas single-void induced C₂₃ and C₅₃ do not as compared in Table 2 by a red frame. Fullerene C₆₀ includes 12 pentagon rings, which suggested us that Band-B may come from multiple pentagon rings. Most chemists think that C₆₀ will be synthesized from small carbon molecules to larger one under heat and catalyst chemical reactions as illustrated on bottom of Fig. 6 by blue panel, which is so called the bottom-up process. Here, we consider reversed process called the top-down process as illustrated in red panel. The top-down process should start from large graphene sheet. This will be attacked by many high-speed particles (red arrows) to create multi-voids. Finally, a graphene sheet transforms to complex graphene molecule having a lot of carbon pentagon rings among hexagon networks. Fullerene C₆₀ may be typical example of such multiple voids induced molecule. Top-down process could be done under low temperature and pure physical quantum-mechanical procedure, which may be popular in space.

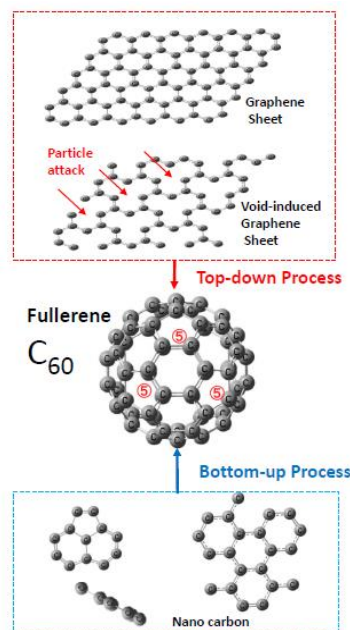


Fig. 6 Top-down and bottom-up process of C₆₀.

4.2 Stable spin state of multi-void induced graphene

To understand the top-down process, we tried simple model starting from C₂₄. Results were summarized in Fig. 7. A single void induced graphene of C₂₃ has one carbon pentagon ring as marked by circled 5. Particle attacks a carbon at red arrowed site. Most stable spin-state was $Sz=2/2$. Two-voids induce C₂₂ having two carbon pentagon rings. Molecular configuration was umbrella like one (see side view). Possible spin states are $Sz=0/2$, $2/2$ and $4/2$. Most stable state was $Sz=2/2$, which energy was 0.17 eV lower than that of $Sz=4/2$ and 1.06 eV lower than $Sz=0/2$. Spin-distribution was illustrated on right. Top carbon of every pentagon ring was up-spin major. Similarly, three voids create C₂₁ having triple carbon pentagons. Stable spin state was $Sz=4/2$.

Size dependence was checked. Large size molecules starting from C₅₄ were analyzed as shown in Fig. 8. Single void induced C₅₃ has stable spin state of $Sz=2/2$. Two voids induced C₅₂ having $Sz=2/2$. Three voids induced C₅₁ having $Sz=2/2$.

In Fig.9, DFT calculated spectra for (C₂₃, $Sz=2/2$), (C₂₂, $Sz=2/2$) and (C₂₁, $Sz=4/2$) were compared. It was a surprise that Band-B (red broken line) was reproduced well by C₂₂ and C₂₁ as the largest band. Astronomically observed Band-B may come from those multi-pentagon rings.

Also in Fig. 10, calculated spectra of C₅₄ family are compared. Major band was just 18.9 μm for both C₅₃ and C₅₂. In case of C₅₁, the largest band was 19.2 μm . However, we could not find any large intensity at 17.4 μm of Band-B. Ratio of number of carbon pentagon rings to hexagons may contribute to the intensity

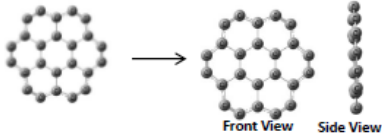
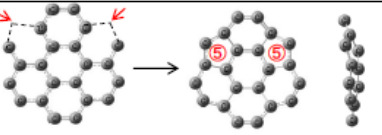
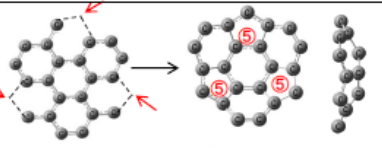
	Initial configuration → Stable configuration	Number of Carbon Rings		Spin State Energy	Stable spin state, Spin-configuration
C_{24}		Hexa.	Penta.	$S_z=2/2$ -2.6eV $S_z=0/2$	$S_z=0/2$ No spin-distribution
C_{23}		6	1	$S_z=0/2$ -0.64eV $S_z=2/2$	$S_z=2/2$ Spin density @10e/nm ² Up-spin, Down-spin Front View, Side View
C_{22}		5	2	$S_z=0/2$ -1.06eV $S_z=4/2$ -0.17eV $S_z=2/2$	$S_z=2/2$ Front View, Side View
C_{21}		4	3	$S_z=6/2$ -1.23eV $S_z=2/2$ -0.16eV $S_z=0/2$ -0.07eV $S_z=4/2$	$S_z=4/2$ Front View, Side View
C_{60}		20	12	$S_z=2/2$ -1.79eV $S_z=0/2$	$S_z=0/2$ No spin-distribution

Fig. 7 Stable spin state of graphene C_{24} family.

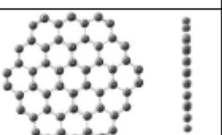
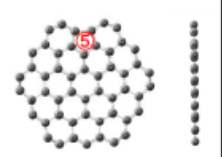
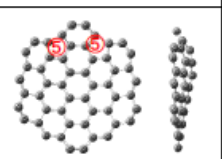
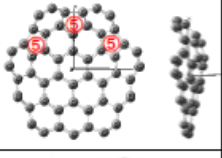
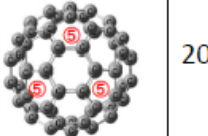
		Carbon Rings		Spin State Energy	Stable spin state, Spin-configuration
C_{54}		Hexa.	Penta.	$S_z=2/2$ Over -2eV $S_z=0/2$	$S_z=0/2$ No spin-distribution
C_{53}		18	1	$S_z=0/2$ -4.2eV $S_z=2/2$	$S_z=2/2$ @10e/nm ³ Front View, Side View
C_{52}		17	2	$S_z=0/2$ -3.2eV $S_z=4/2$ -0.16eV $S_z=2/2$	$S_z=2/2$ Front View, Side View
C_{51}		16	3	$S_z=0/2$ +0.10eV $S_z=4/2$ -0.06eV $S_z=2/2$	$S_z=2/2$ Front View, Side View
C_{60}		20	12	$S_z=2/2$ -1.79eV $S_z=0/2$	$S_z=0/2$ No spin-distribution

Fig. 8 Stable spin state of C_{54} family.

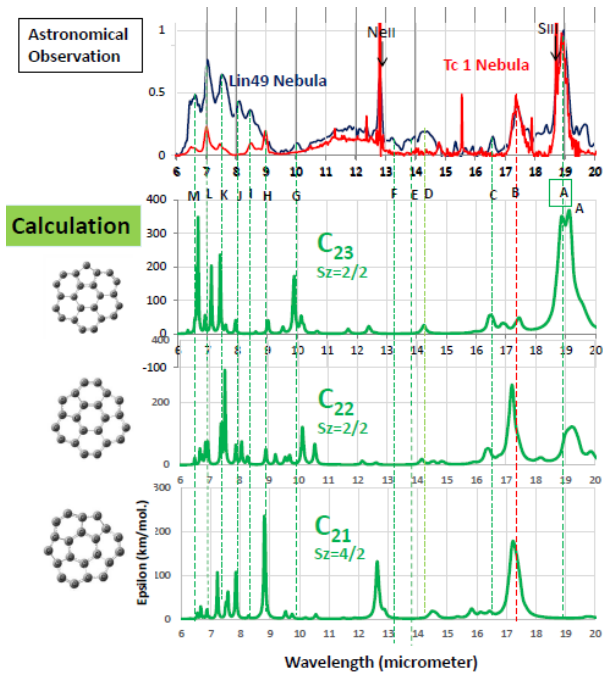


Fig. 9 DFT calculated spectra of (C_{23} , $S_z=2/2$), (C_{22} , $S_z=2/2$) and (C_{21} , $S_z=4/2$) compared with astronomically observed ones.

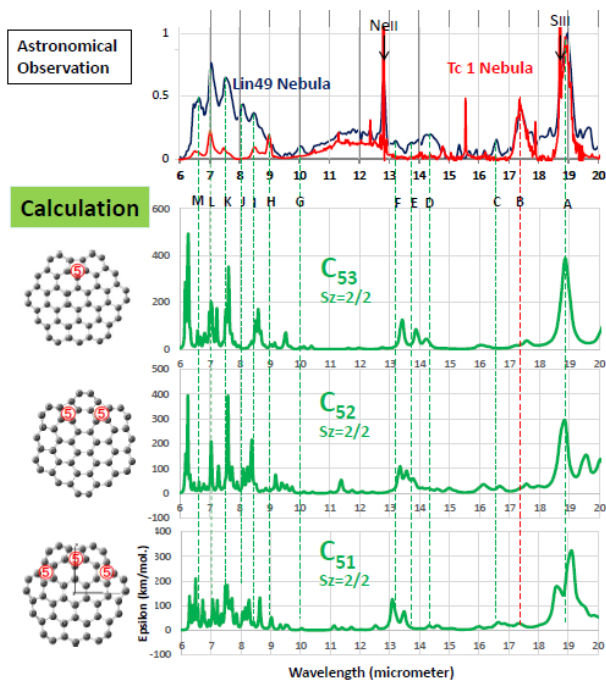


Fig. 10 DFT calculated spectra of (C_{53} , $S_z=2/2$), (C_{52} , $S_z=2/2$) and (C_{51} , $S_z=2/2$) compared with astronomically observed ones.

5. Reproduction of astronomically observed spectrum.

We tried to reproduce astronomically observed spectrum using DFT spectra of C_{60} and graphene molecules. As shown in Fig. 11, observed spectrum of Tc1 in panel (A) could be reproduced fairly well by C_{60} in panel (C). It should be minded that Band-H and K of Tc1 could not reproduced by C_{60} . Observed spectrum of Lin49 in (B) is so complex, could not be reproduced only by C_{60} . Here, we obtained simple weighting sum of DFT calculated spectrum of graphene molecules of C_{23} , C_{22} , C_{53} , and C_{52} as shown in (D). Observed major bands of Band-A and B were well reproduced. Also detailed bands of Band-C, D, E, F, were reproduced well. Further, shorter wavelength bands (Band-G, I, K, L and M) were also well reproduced again. Here, we add a DFT spectrum of C_{60} to graphene as illustrated in (E). It looks that major part are similar with (D), may come from graphene molecules.

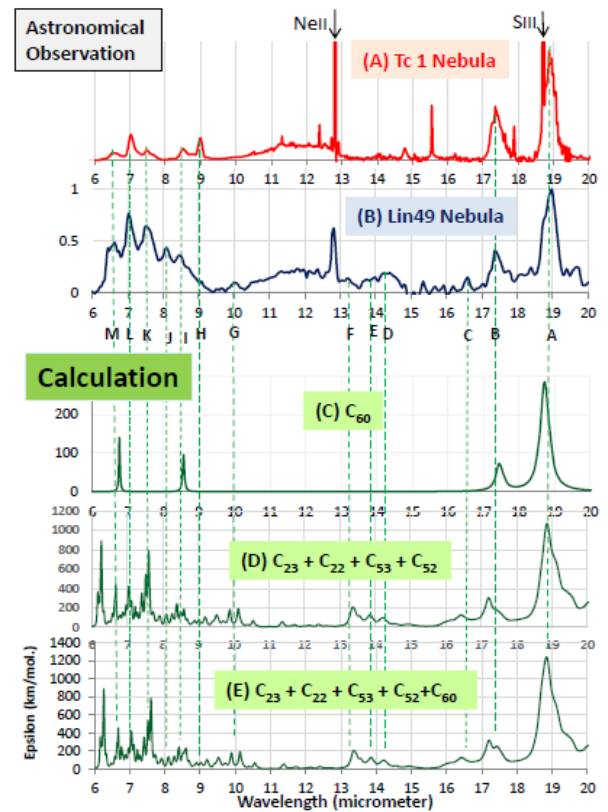


Fig. 11 DFT calculated molecular vibrational spectrum is shown compared with astronomical observation of Tc1 nebula on (A) and Lin49 on (B). DFT calculated spectrum of C_{60} was shown in (C). Simple sum spectrum of C_{23} , C_{22} , C_{53} and C_{52} is illustrated on (D). Further addition of C_{60} is on (E).

5. Conclusion

Stable spin state and molecular vibrational infrared spectrum of fullerene C₆₀ was studied comparing with void induced graphene molecules.

- (1) Spin state of fullerene C₆₀ were calculated by DFT to result that stable one was non-magnetic of $S_z=0/2$. This is contrary to graphene molecules of C₂₃ and C₅₃ to be magnetic $S_z=2/2$.
- (2) Spin alignment model by two graphene molecules suggested that up-spin on each carbon pentagon ring cancel each other to bring up-down spin pair to be non-magnetic $S_z=0/2$. There may occur similar cancelation in C₆₀.
- (3) Simulated molecular vibrational infrared spectrum of C₆₀ show four modes, which coincide well with laboratory experiment of gas-phase emission spectrum. Also, those coincide well with astronomically observed bands of nebula Tc1 and Lin49.
- (4) There remain unidentified astronomical bands. Multiple voids induced graphene were studied. Two voids induced C₂₂ having two pentagon rings could reproduce remained and detailed astronomical observation.
- (5) Simple sum of DFT calculated spectra by C₆₀ and graphene molecules (C₂₃, C₂₂, C₅₃ and C₅₂) could successfully reproduce astronomical bands in detail.

Acknowledgement Aigen Li is supported in part by NSF AST-1311804 and NASA NNX14AF68G.

References

(Note on abbreviation of astronomical journals,

ApJ: The Astrophysical Journal

ApJL: The Astrophysical Journal Letters

A&A: Astronomy and Astrophysics

MNRAS: Monthly Notices of the Royal Astronomical Society

PNAS: Proceedings of the National Academy of Sciences)

- 1) P. Esquinazi, D. Spemann, R. Hohne, A. Setzer, K. Han, and T. Butz: *Phys. Rev. Lett.*, **91**, 227201 (2003).
- 2) K. Kamishima, T. Noda, F. Kadonome, K. Kakizaki and N. Hiratsuka: *J. Mag. Magn. Mat.*, **310**, e346 (2007).
- 3) T. Saito, D. Nishio-Hamane, S. Yoshii, and T. Nojima: *Appl. Phys. Lett.*, **98**, 052506 (2011).
- 4) Y. Wang, Y. Huang, Y. Song, X. Zhang, Y. Ma, J. Liang and Y. Chen: *Nano Letters*, **9**, 220 (2009).
- 5) J. Cervenka, M. Katsnelson and C. Flipse: *Nature Phys.*, **5**, 840 (2009), (<https://doi.org/10.1038/nphys1399>).
- 6) H. Ohldag, P. Esquinazi, E. Arenholz, D. Spemann, M. Rothermal, A. Setzer, and T. Butz: *New Journal of Physics*, **12**, 123012 (2010).
- 7) J. Coey, M. Venkatesan, C. Fitzgerald, A. Douvalis and I. Sanders: *Nature*, **420**, 156 (2002).
- 8) K. Kusakabe and M. Maruyama: *Phys. Rev. B*, **67**, 092406 (2003).
- 9) N. Ota, N. Gorjizadeh and Y. Kawazoe: *J. Magn. Soc. Jpn.*, **35**, 414 (2011), also **36**, 36 (2012).
- 10) N. Ota: *J. Magn. Soc. Jpn.*, **37**, 175 (2013).
- 11) P. Lehtinen, A. Foster, Y. Ma, A. Krasheninnikov, and R. Nieminen: *Phys. Rev. Lett.*, **93**, 187202 (2004).
- 12) P. Ruffieux, O. Groning, P. Schwaller, L. Schlapbach, and P. Groning: *Phys. Rev. Lett.*, **84**, 4910 (2000).
- 13) A. Hashimoto, K. Suenaga, T. Sugai, H. Shinohara, and S. Iijima: *Nature (London)*, **430**, 870 (2004).
- 14) K. Kelly and N. Hales: *Sur. Sci.*, **416**, L1085 (1998).
- 15) T. Kondo, Y. Honma, J. Oh, T. Machida, and J. Nakamura: *Phys. Rev. B*, **82**, 153414 (2010).
- 16) M. Ziatdinov, S. Fujii, K. Kusakabe, M. Kiguchi, T. Mori, and T. Enoki: *Phys. Rev. B*, **89**, 155405 (2014).
- 17) N. Ota and L. Nemes: *J. Magn. Soc. Jpn.*, **45**, 30 (2021).
- 18) K. Kelly and N. Hales: *Sur. Sci.*, **416**, L1085 (1998).
- 19) T. Kondo, Y. Honma, J. Oh, T. Machida, and J. Nakamura: *Phys. Rev. B*, **82**, 153414 (2010).
- 20) M. Ziatdinov, S. Fujii, K. Kusakabe, M. Kiguchi, T. Mori, and T. Enoki: *Phys. Rev. B*, **89**, 155405 (2014).
- 22) O. Yazyev and L. Helm: *Phys. Rev. B*, **75**, 125408 (2007).
- 23) B. Wang and S. Pantelides: *Phys. Rev. B*, **86**, 165438 (2012).
- 24) N. Ota, A. Li, L. Nemes and M. Otsuka: *J. Magn. Soc. Jpn.*, **45**, 41 (2021).
- 25) M. Otsuka, F. Kemper, M. L. Leal-Ferreira, M. L. Aleman, M. L. Bernard-Salas, J. Cami, B. Ochsendorf, E. Peeters, and P. Scicluna: *MNRAS*, **462**, 12 (2016).
- 26) L. Nemes, E. Brown, S. C. Yang, U. Hommerich: *Spectrochimica Acta Part A, Molecular and Biomolecular Spectroscopy*, **170**, 145 (2017).
- 27) L. Nemes, R. S. Ram, P. F. Bernath, F. A. Tinker, M. C. Zumwalt, L. D. Lamb, D. R. Huffman: *Chem. Phys. Lett.*, **218**, 295 (1994).
- 28) W. Kratschmer, L. D. Lamb, K. Fostiropoulos and D. R. Huffman: *Nature*, **347**, 354 (1990).
- 29) L. Nemes, A. Keszler, J. Hornkohl, and C. Parigger: *Applied Optics*, **44-18**, 3661 (2005).
- 30) H. W. Kroto, J. R. Heath, S. C. O'Brien, R. F. Curl, and R. E. Smalley: *Nature*, **318**, 162 (1985).
- 31) J. Cami, J. Bernard-Salas, E. Peeters and S. E. Malek: *Science*, **329**, 1180 (2010).
- 32) K. Sellgren, M. W. Werner, J. G. Ingalls, J. D. T. Smith, T. M. Carleton and J. Christine: *ApJL*, **722**, L54 (2010).
- 33) Y. Zhang, & S. Kwok: *ApJ*, **730**, 126 (2011).
- 34) O. Bern' e & A. G. G. M. Tielens: *PNAS*, **109**, 4010 (2012) Also, Bern' e, N. L. J. Cox, G. Mulas & C. Joblin: *A&A*, **605**, L1 (2017).
- 35) D. A. Garc'ia-Hern'andez, A. Manchado, P. Garc'ia-Lario, et al.: *ApJL*, **724**, L39 (2010).
- 36) M. C. Martin, D. Koller, and L. Mihaly: *Phys. Rev.* **B47**, 14607 (1993).
- 37) J. Fabian: *Phys. Rev.* **B53**, 13864 (1996).
- 38) A. Candian, M. G. Rachid, H. MacIssac, V. N. Staroverov, E. Peeters, and J. Cami: preprint from web site of *ResearchGate* by Alessandra Candians, titled "Searching

- for stable fullerenes in space with computational chemistry” (2009).
- 39) H.W. Kroto & K. McKay: *Nature*, **331**, 328 (1988).
- 40) A. Chuvilin, U. Kaiser, E. Bichoutskaia, N. A. Besley, & A.N. Khlobystov: *Nature Chem.*, **2**, 450 (2010).
- 41) A. K. Geim & K. S. Novoselov: *Nature Materials*, **6**, 183 (2007).
- 42) D. A. Garcia-Hernandez, Rao N. Kameswara & D. L. Lambert: *ApJ*, **729**, 126 (2011).
- 43) D. A. Garcia-Hernandez, S. Iglesias, J. A. Acosta-Pulido, et al.: *ApJL*, **737**, L30 (2011).
- 44) D. A. Garcia-Hernandez, E. Villaver, P. Garc’ia-Lario, et al.: *ApJ*, **760**, 107 (2012).
- 45) C. Duboscq, F. Caldvo, M. Rapacioli, E. Dartois, T. Pino, C. Falvo, and A. Simon: *A&A*, **634**, A62 (2020).
- 46) N. Ota: *arXiv*, 1412.0009 (2014), Additional data for scaling factor on *arXiv*, 1502.01766,
- for emission spectrum calculation on *arXiv*, 1703.05931, for SP3 defect mechanism on *arXiv*, 1808.01070.
- 47) H. Galue, and G. Leines: *Phys. Rev. Lett.*, **119**, 171102 (2017).
- 48) P. Hohenberg and W. Kohn: *Phys. Rev.*, **136**, B864 (1964).
- 49) W. Kohn and L. Sham: *Phys. Rev.*, **140**, A1133 (1965).
- 50) A. Becke: *J. Chem. Phys.*, **98**, 5648 (1993).
- 51) M. Frisch, G. Trucks, H. Schlegel et al: Gaussian 09 package software, Gaussian Inc. Wallington CT USA (2009).
- 52) R. Ditchfield, W. Hehre and J. Pople: *J. Chem. Phys.*, **54**, 724(1971).
- 53) B. T. Draine and A. Li: *ApJ*, **551**, 807 (2001).
- 54) A. Li and B. T. Draine: *ApJ*, **554**, 778 (2001).